doi:10.3772/j.issn.1006-6748.2015.02.014

RF energy harvesting system for wireless intraocular pressure monitoring①

Liu Demeng (刘德盟)[*,**], Mei Niansong[*], Zhang Zhaofeng②[*]
([*] Micro-Nano Device Research Center, Shanghai Advanced Research Institute, Chinese Academy of Science, Shanghai 201210, P. R. China)
([**] University of Chinese Academy of Sciences, Beijing 100049, P. R. China)

Abstract

This paper presents an RF energy harvesting system for wireless intraocular pressure monitoring applications. The system consists of an implantable antenna and a rectifier. A new sizing strategy is adopted to optimize the conversion efficiency of the rectifier, and the design principle of an implantable antenna is introduced from material selection and structure design. Results from testing demonstrate that the antenna gain is about −20 dBi and the rectifier's maximum total conversion efficiency which contains match efficiency and rectifying efficiency is 47.18% under the implementation of 0.18μm standard CMOS process. The maximum power obtained from the proposed system is 8μW when the power density of electromagnetic wave is lower than the national standard 40μW/cm^2 at 915MHz, which is enough to power the intraocular pressure monitoring system.

Key words: RF energy harvesting system, implantable medical system, antenna, rectifier, intraocular pressure monitoring

0 Introduction

Glaucoma is one of the leading causes of blindness, impacting about 8.4 million people worldwide[1]. Continuous measurement of intraocular pressure in anterior chamber is an important pathway in the diagnosis and treatment of glaucoma[2]. Implantable intraocular pressure monitoring system has been developed to finish the pressure continuous measurement[3-5]. Because of the limit of the volume of anterior chamber and long term working, passive structures are usually adopted. An energy harvesting system is used to extract power from the transmitted RF energy.

The function of the RF energy harvesting system is to convert RF energy to usable DC power. RF energy harvesting system has captured many research interests in applications such as wireless sensor network (WSN)[6-9] and medical electronics[10]. The RF energy harvesting system used in implantable medical takes more challenge than this system used in WSN. Due to the tissue attenuation, high power conversion efficiency is hard to be achieved.

The system consists of an antenna for picking up power radiated by the RF waves, a conjugate impedance match ensuring maximum power transfer in the system, and a rectifier circuit for converting the RF energy to a DC power. The harvesting energy of the system depends on the gain of the received antenna, the matched-degree of impedance match and the rectifier efficiency. In order to make the RF energy harvesting system to obtain enough energy to power the implantable system, this paper focuses on a relatively high gain implantable antenna, a new method of the rectifier efficiency and impedance matching efficiency designing separately and a new sizing strategy to improve efficiency of rectifier.

This paper is organized as follows. Section 1 introduces the system link calculation. Section 2 shows the design of the antenna. Section 3 discusses the principles and design of high efficiency differential drive CMOS rectifier. Section 4 shows the photograph of the RF energy harvesting system and describes the experimental results. Finally, conclusions are given in Section 5.

1 System link budget

System design begins with life safety requirement, which requires the electromagnetic wave power density is lower than the national standard 40μW/cm^2 at 915MHz for safety levels with respect to human expo-

① Supported by the Shanghai Science Committee Project (No. Y232821D01).
② To whom correspondence should be addressed. E-mail: zhangzf@sari.ac.cn
Received on Feb. 27, 2014

sure to radio frequency electromagnetic fields[11]. The distance of the reader and the implantable system is 5cm which is enough for this application and some assumption is taken from previous studies as below: the gain of the implantable antenna is −20dBi, the impedance match efficiency is 0.8, and the efficiency of the rectifier is 50%, the extra loss of EM wave in air is 0.5dB.

Firstly, we calculate that the maximum delivered power of the reader is 11dBm from the equations below:

$$S = \frac{P_t G_t}{4\pi R^2} = \frac{P_{EIRP}}{4\pi R^2} \quad (1)$$

$$P_{DC} = P_{EIRP} G_{ana} \left(\frac{\lambda}{4\pi R}\right)^2 \rho\sigma \quad (2)$$

The output DC power of the energy harvesting system is expressed in Eq. (2), where P_{EIRP} is the emission power density of the reader, G_{ana} is the gain of the implantable antenna, $(\lambda/4\pi R)^2$ is the radiation loss, ρ is the efficiency of impedance match and σ is the efficiency of the rectifier. The calculated results are as below: the radiation loss is −5.65dB, the available power of the antenna is 4.85dBm, and the received power of the antenna is −15.62dBm, the DC power of the energy harvesting system is about 10.96μW, which is higher than the requirement of the implantable pressure monitoring 2.3μW[3].

2 Antenna design

2.1 Frequency selection

The main effects of the implanted antenna are a reduction of its dimension and an increase on the propagation loss. These effects are mainly due to the high permittivity and high conductivity of the human eye tissues. The propagation loss in a link between an implanted antenna and an external antenna has been evaluated at the ISM bands of 433MHz, 915MHz, 2450MHz and 5800MHz[12], the conclusion shows that the lower the frequency, the higher the pair gain. A clear tradeoff between antenna dimensions and performance exists. When the frequency increases, antenna dimension is reduced, but the antenna pair gain decreases and it degrades the system performance. According to the results of Ref. [12], the band of 915MHz is most suitable to be chosen as the wireless transmission frequency, as the dimension of antenna at 915MHz can be implemented in anterior chamber.

2.2 Material selection

The biocompatible material which takes no harm to human tissues is chosen to fabricate the implanted pressure system so that long-term monitoring of glaucoma patients can be fulfilled, such as PMMA[3,13,14], Parylene C[15-17], PDMS[18] and liquid-crystal polymer (LCP)[5]. Among these materials, Parylene and PDMS are soft material, having strong water permeability. The conductivity and permittivity of the material change when water permeates into. The performance of the antenna then decreases. Therefore PMMA is the most suitable material, and it is used in this design.

2.3 Structure design

The structure of the implanted antenna is designed based on the human anterior chamber environment. As Fig. 1 shows, the central hole of the loop antenna is designed to avoid the quantity of light into the pupil decreasing. As the diameter of pupil changes from 2.5mm to 4mm normally, the diameter of the central hole is 5mm. As the diameter of anterior chamber is about 12.11mm, the diameter of the antenna is designed to be 11.4mm. The antenna uses copper as the conductive material. The thickness of the antenna is about 0.1mm.

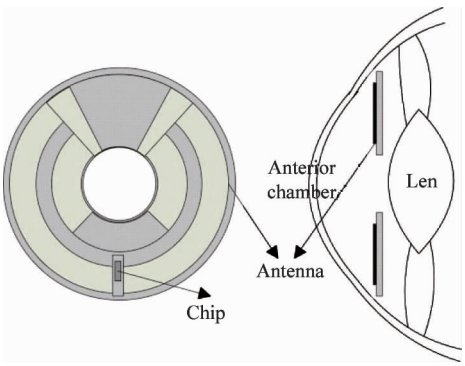

Fig. 1 Structure of the implanted antenna and location of the implanted system

The antenna is a dipole-like structure and modeled using Ansoft's high frequency structural simulator (HFSS) in eye tissue, as Fig. 2(a) shows. In order to obtain the precise simulation results of the implanted antenna, human eye and adjacent tissue are modeled by HFSS with empirically measured material properties of permittivity and conductivity[19]. The antenna shape and dimensions are chosen based on clinical requirements and then adjusted and optimized for electromagnetic performance. Fig. 2(b) shows that the simulated gain of the antenna is about −17dBi, and the S11 parameter is about −30dB, as Fig. 2(c) shows, the impedance matches to $30 - j115\ \Omega$, which is the input impedance of the rectifier.

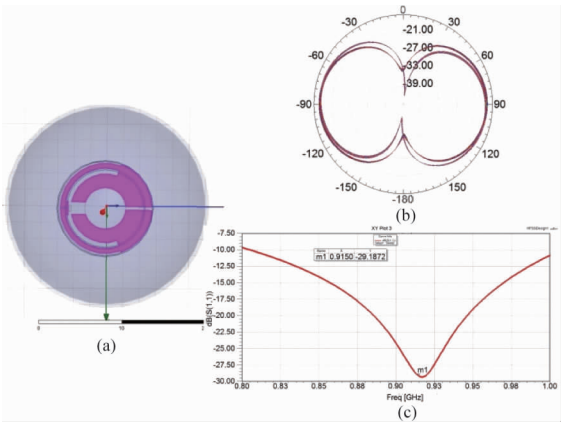

Fig. 2 Structure of the antenna in HFSS (a) and the simulation result of gain (b) and S11 parameter(c)

3 Rectifier design

3.1 Topology selection

Power conversion efficiency (PCE) of the rectifier circuit is defined by the output power divided by the input power. The improvement of PCE is an effective approach to improve the output power of the harvesting system. The PCE of the rectifier circuit is affected by circuit topology. There are several topologies used in the rectifier, such as: basic diode-connected MOSFET rectifier[20], zero-V_{th} diode-connected MOSFET rectifier[21], schottky diodes rectifier[22], static conduction voltage cancellation rectifier[23] and active conduction voltage cancellation rectifier[24]. Among these topologies, zero-V_{th} diode-connected MOSFET and schottky diodes rectifier need additional process in custom CMOS process and the cost will increase. Active conduction voltage cancellation rectifier has larger PCE than basic diode-connected MOSFET rectifier and static conduction voltage cancellation rectifier. In this paper, active conduction voltage cancellation topology is used in designing the rectifier.

3.2 Efficiency analysis

Fig. 3 (a) shows the 2-stages active conduction voltage cancellation differential-drive CMOS rectifier circuit, which has a cross-coupled differential CMOS configuration with a bridge structure. Transient and AC analysis are taken in order to find the optimization functions of PCE and input impedance. As PCE can be expressed as below:

$$PCE = \frac{P_{DC}}{P_{DC} + P_{loss}} \tag{3}$$

where P_{DC} means the DC power of the load impedance, and P_{loss} contains two parts: power loss of the turn-on resistance of the MOSFET and leakage power, and the leakage power is much smaller than the power loss of the turn-on resistance.

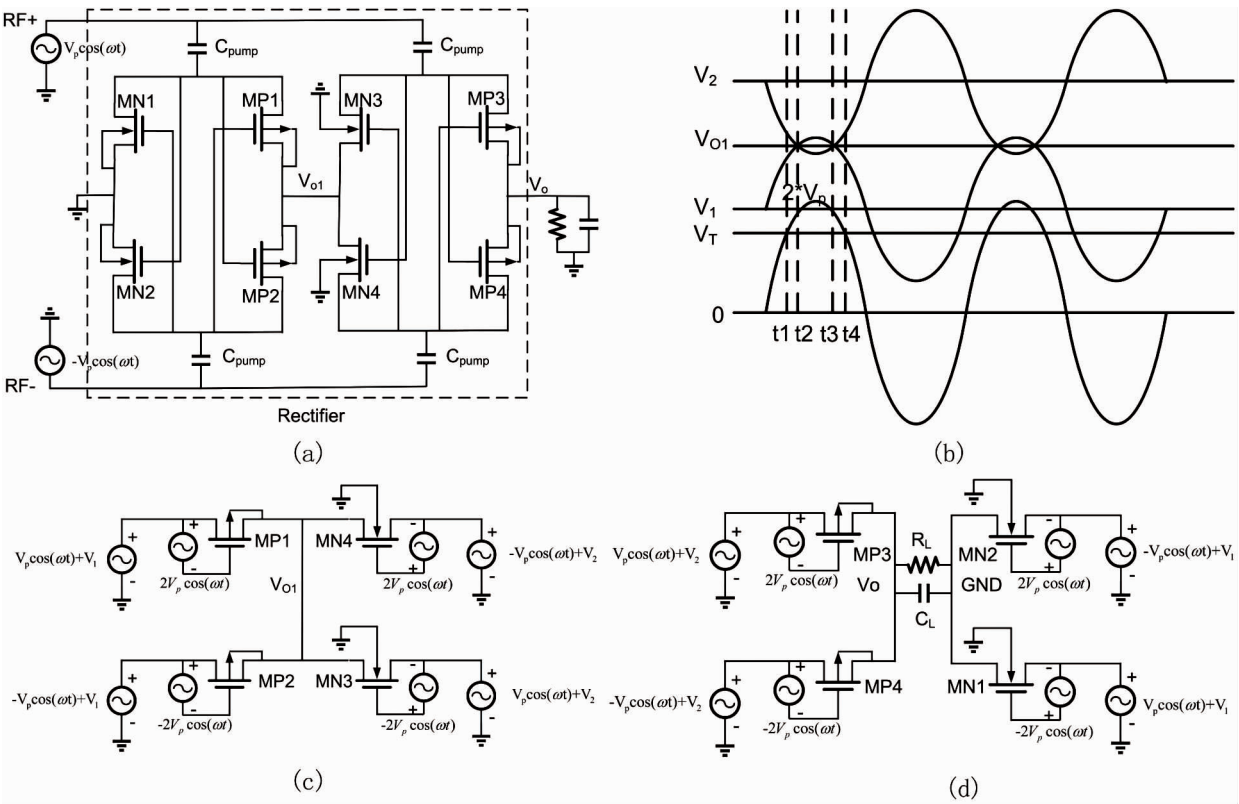

Fig. 3 The circuit structure of the proposed rectifier (a) and voltage waveform of the main node voltage (b) and transient analysis equivalent circuit of the rectifier circuit with 2 stages (c) (d)

Table 1 The working conditions of MP1 and MN4

Time	MP1			MN4		
	$\lvert V_{gs}\rvert$	V_{ds}	V_T	V_{gs}	V_{ds}	V_T
$t1 < t < t2$, $t3 < t < t4$	$V_{o1} - V_1 + V_p\cos(\omega t)$	$V_{o1} - V_1 - V_p\cos(\omega t)$	V_{tp0}	$V_2 + V_p\cos(\omega t) - V_{o1}$	$V_2 - V_p\cos(\omega t) - V_{o1}$	$V_{tn0} + \gamma(\lvert 2\Phi_F + V_{o1}\rvert^{1/2} - \lvert 2\Phi_F\rvert^{1/2})$
$t2 < t < t3$	$2V_p\cos(\omega t)$	$V_1 + V_p\cos(\omega t) - V_{o1}$	$V_{tp0} + \gamma(\lvert 2\Phi_F + V_1 + V_p\cos(\omega t) - V_{o1}\rvert^{1/2} - \lvert 2\Phi_F\rvert^{1/2})$	$2V_p\cos(\omega t)$	$V_{o1} - V_2 + V_p\cos(\omega t)$	$V_{tn0} + \gamma(\lvert 2\Phi_F + V_2 - V_p\cos(\omega t)\rvert^{1/2} - \lvert 2\Phi_F\rvert^{1/2})$

The transient analysis equivalent circuit of the rectifier under quasi-steady state is shown in Fig. 3(c) and (d). Fig. 3 (b) shows the voltage waveform of the main node voltage. The output voltage of each stage is approximately fixed voltage source. There are twice conductions in each period from RF + to RF −: from MP1 to MN4 and from MP2 to MN3 in the first stage. Table 1 shows the working conditions of MP1 and MN4, the conditions of MP2 and MN3 are the same with MP1 and MN4, and among these parameters of Table 1, V_p is related to the energy of which the rectifier obtains from RF and the input impedance of the rectifier, and $V_{o1} = V_o/N$, where N is the number of the rectifier stage. The analysis of the other stage is similar to the first stage.

As the current of MP1 and MN4 is equivalent in each conduction period, the equation is shown as follows:

$$\int_{t_{1p}}^{t_{4p}} (V_p\cos(\omega t) + V_1 - V\,O1)/R_{on,MP1}\,dt = \int_{t_{1n}}^{t_{4n}} (V_{O1} + V_p\cos(\omega t) - V_2)/R_{on,MN4}\,dt \quad (4)$$

$$2 \times \int_{t_{1p}}^{t_{4p}} (V_p\cos(\omega t) + V_2 - V_O)/R_{on,MP3}\,dt = 2 \times \int_{t_{1n}}^{t_{4n}} (V_p\cos(\omega t) - V_1)/R_{on,MN2}\,dt \quad (5)$$

And P_{loss} in each period can be found as follows:

$$P_{loss} = 2 \times \{\int_{t_{1p}}^{t_{4p}} (V_p\cos(\omega t) + V_1 - V_{O1})^2/R_{on,MP1}\,dt + \int_{t_{1n}}^{t_{4n}} (V_{O1} + V_p\cos(\omega t) - V_2)^2/R_{on,MN4}\,dt\} + 2 \times \int_{t_{1p}}^{t_{4p}} (V_p\cos(\omega t) + V_2 - V_O)^2/R_{on,MP3}\,dt + 2 \times \int_{t_{1p}}^{t_{4p}} (V_p\cos(\omega t) - V_1)^2/R_{on,MN2}\,dt \quad (6)$$

We can draw the conclusion that PCE depends on the V_o, N, V_p and the dimension of MOSFET. Two stages rectifier is selected as the example to analyze the rectifier above.

3.3 Impedance analysis

The AC analysis is taken to obtain the input impedance, the AC equivalent circuit is shown in Fig. 4(a), where the parameter is expressed as follows: $C_1 = C_{gs,MP1} + C_{gs,MN2}$, $R_1 = R_{ON,MP1} + R_{ON,MN4}$, $C_2 = C_{gs,MP3} + C_{gs,MN4}$, $R_2 = R_{ON,MP3} + R_{ON,MN2}$. And the input impedance can be expressed as bellow:

$$Z_{in} = \left(\frac{2}{sC_{pump}} + \frac{1}{sC_1}//R_1\right) //\left(\frac{2}{sC_{pump}} + \frac{1}{sC_2}//\left(R_2 + R_L//\frac{1}{sC_L}\right)\right) \quad (7)$$

where C_1 and C_2 depend on the dimension of MOSFET, R_1 and R_2 depend on the dimension of MOSFET and input power, R_{on} decreases when the input power increases. So when the dimension of MOSFET is fixed, Z_{in} changes with the input power. Fig. 4(b) shows the change of real part and image part of Z_{in} with R_{on}. Fig. 4(c) shows the change of Z_{in} with frequency and the calculation conditions are that: $C_{pump} = 1.2$pF, $C_L = 10$pF, $R_L = 75$kΩ.

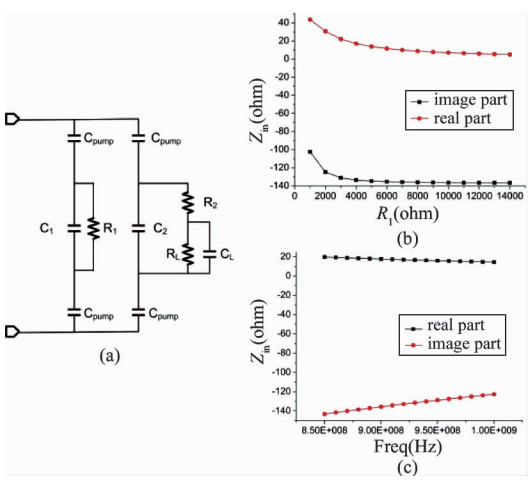

Fig. 4 (a) AC equivalent circuit for the input impedance, (b) the change of Z_{in} with R_{on}, (c) the change of Z_{in} with frequency

3.4 Optimal design

Cadence Spectre is used to simulate the rectifier based on the analysis above. As we know from the efficiency analysis, more power will loose on the R_{on} as the larger number N of the rectifier stages. Since the implantable system always works under the low supply voltage, a rectifier with 2-stages produces enough voltage to power it. Then we increase the W/L of MOSFET of the first stage to increase rectifier efficiency, but the maximum efficiency would keep constant when the size of MOSFET is bigger than a certain degree, because the reduction of the power loss on R_{on} is not obvious when the W/L ratio of MOSFET is larger than a certain lever, and more leak current occurs with the higher W/L ratio. Fig. 5 (a) shows the efficiency changing with the input peak voltage V_p in different W/L ratio. Fig. 5 (b) shows the result of the impedance match efficiency and rectifier efficiency changing with input power. The maximum rectifying efficiency is about 80%, and the maximum match efficiency is only 83% because of the large signal input impedance match loss.

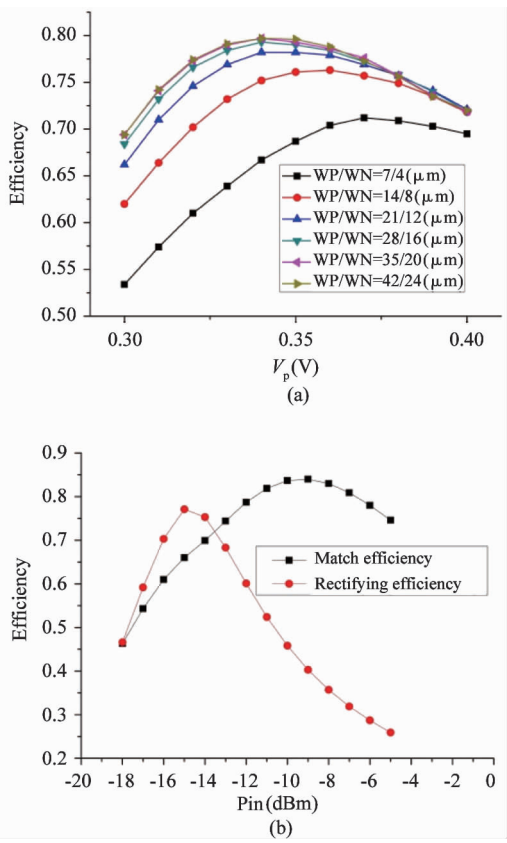

Fig. 5 (a) The rectifier efficiency changes with the input peak voltage V_p in different W/L, (b) The rectifying efficiency and match efficiency in different Pin

4 Experimental results

4.1 Test results of the rectifier

The evaluation of the implanted antenna performance is difficult because it is almost impossible to make antenna measurements in the real operating scenario (inside the human eye). The performance of the rectifier is measured to verify its design, then the system which contains antenna and rectifier is tested.

Fig. 6 shows the photograph of the proposed RF energy harvesting system, and the dimension of the antenna has been described in Section 2. The rectifier is fabricated in a 0.18μm 2 P4M standard CMOS process, and the die area is $250 \times 200 \mu m^2$.

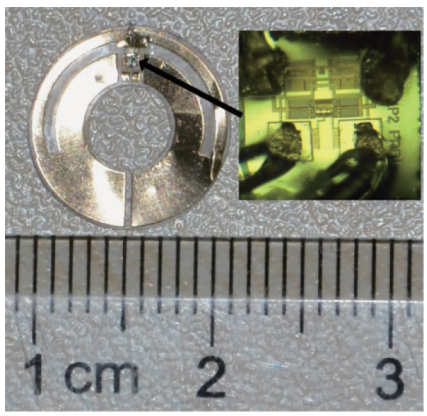

Fig. 6 Photograph of the proposed RF energy harvesting system

Fig. 7 (a) shows the test result of the input impedance of the rectifier in the input power range from −14dBm to 7dBm. The image part of the input impedance keeps constant, and the real part increases with the input power, the reason is that the R_{on} of MOSFET decreases with the input power. The input impedance is measured by network analyzer. Fig. 7 (b) shows the changes of the total rectifier efficiency with input power. The test conditions are set as below: the load impedance is 75kΩ, and the load capacitance is 10pF. The total efficiency is the result of the rectifier efficiency multiplied by the impedance match efficiency, and the maximum test efficiency is 47.18%. Agilent Analog Signal Generator E8257D is used to power the rectifier. A balun converts the single-ended signal to the differential one. There are some factors which cause the reduction of the rectifier's received power, such as insertion loss of balun and SMA connector, power loss of the PCB, etc. Therefore the measured efficiency is a little bit lower than the simulated efficiency in Fig. 7 (b).

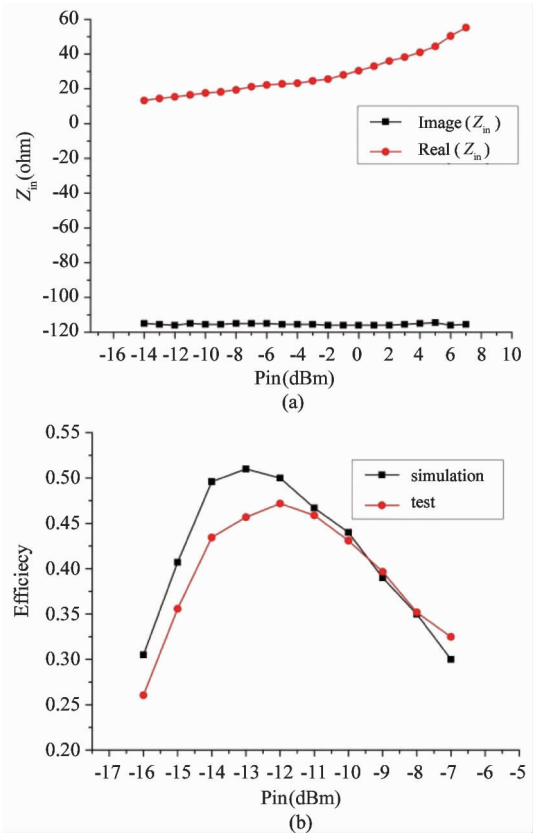

Fig. 7 The test results of the input impedance (a) and total efficiency (b)

4.2 Test results of the system

Fig. 8(a) shows the power obtained by the RF energy harvesting system in different frequency. The test conditions are set as below: the output power of the reader is 11dBm, the distance between the reader and implanted system is 5cm, and the RF harvesting system is placed in anterior chamber of pig, the load impedance is 75kΩ. The test results show that the maximum converted power is about 8μW, which is lower than the analysis of Section 1. This is caused by extra EM absorption and reflection in multilayered medium. If the total efficiency of rectifier is 40%, then we can deduce that the gain of the antenna is about −20dBi. Fig. 8(b) shows the DC power of the RF harvesting system in different output power of the reader.

5 Conclusion

An RF energy harvesting system for intraocular pressure monitoring is proposed in this paper. An implantable antenna, a rectifier and impedance matching between antenna and rectifier are designed respectively for higher RF energy conversion efficiency. The proposed system is tested in biological environment and the DC power obtained from this system is about 8μW.

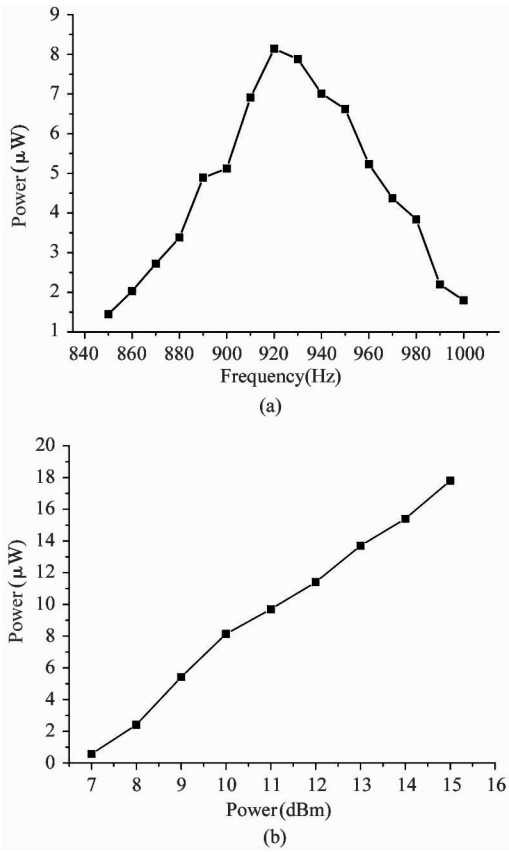

Fig. 8 DC power of the RF energy harvesting system in different frequency (a) and in different input power (b)

References

[1] Quigley H, Broman A. The number of people with glaucoma worldwide in 2010 and 2020. *British Journal of Ophthalmology*, 2006, 90(3): 262-267

[2] Katuri K C, Asrani S, Ramasubramanian M K. Intraocular pressure monitoring sensors. *IEEE Sensors Journal*, 2008, 8(1): 12-19

[3] Shih Y C, Shen T, Otis B. A 2.3μW wireless intraocular pressure/temperature monitor. *IEEE Journal of Solid-State Circuits*, 2011, 46(11): 1-4

[4] Chen G, Ghaed H, Haque R, et al. A cubic-millimeter energy-autonomous wireless intraocular pressure monitor. In: Proceedings of the IEEE International Solid-State Circuits Conference Digest of Technical Papers (ISSCC), San Francisco, USA, 2011. 310-312

[5] Chow E Y, Chlebowski A L, Irazoqui P P. A miniature-implantable RF-wireless active glaucoma intraocular pressure monitor. *IEEE Transactions on Biomedical Circuits and Systems*, 2010, 4(6): 340-349

[6] Le T, Mayaram K, Fiez T. Efficient far-field radio frequency energy harvesting for passively powered sensor networks. *IEEE Journal of Solid-State Circuits*, 2008, 43(5): 1287-1302

[7] Dowling J, Tentzeris M M, Beckett N. RFID-enabled temperature sensing devices: A major step forward for energy efficiency in home and industrial applications? In:

Proceedings of the IEEE MTT-S International Microwave Workshop on Wireless Sensing, Local Positioning, and RFID, Cavtat, Croatia, 2009. 1-4

[8] Vyas R, Lakafosis V, Tentzeris M, et al. A battery-less, wireless mote for scavenging wireless power at UHF (470-570 MHz) frequencies. In: Proceedings of the 2011 IEEE International Symposium on Antennas and Propagation (APSURSI), Spokane, USA, 2011. 1069-1072

[9] Stoopman M, Keyrouz S, Visser H J, et al. Co-design of a CMOS rectifier and small loop antenna for highly sensitive RF energy harvesters. *IEEE Journal of Solid-State Circuits*, 2014, 49(3): 622-634

[10] Le H, Fong N, Luong H C. RF energy harvesting circuit with on-chip antenna for biomedical applications. In: Proceedings of the 2010 Third International Conference on Communications and Electronics (ICCE), Nha Trang, Vietnam, 2010. 115-117

[11] Ministry of Environmental Protection of the People's Republic of China. GB8703-88 Regulations for Electromagnetic Radiation Protection. Beijing, China: Standards Press of China, 1988 (In Chinese)

[12] Gemio J, Parron J, Soler J. Human body effects on implantable antennas for ISM bands applications: Models comparison and propagation losses study. *Progress In Electromagnetics Research*, 2010, 110: 437-452

[13] Puers R, Vandevoorde G, Bruyker D D. Electrodeposited copper inductors for intraocular pressure telemetry. *Journal of Micromechanics and Microengineering*, 2000, 10: 124-129

[14] Eggers T, Draeger J, Hille K, et al. Wireless intra-ocular pressure monitoring system integrated into an artificial lens. In: Proceedings of the 1st Annual International Conference On Microtechnologies in Medicine and Biology, Lyon, France, 2000. 466-469

[15] Chen P J, Rodger D C, Humayun M S, et al. Unpowered spiral-tube parylene pressure sensor for intraocular pressure sensing. *Sensors and Actuators A: Physical*, 2006, 127(2): 276-282

[16] Chen P J, Rodger D C, Saati S, et al. Microfabricated implantable parylene-based wireless passive intraocular pressure sensors. *Journal of Microelectromechanical Systems*, 2008, 17(6): 1342-1351

[17] Chen P J, Rodger D C, Saati S, et al. Implantable parylene-based wireless intraocular pressure sensor. In: Proceedings of the 21st IEEE International Conference on Micro Electro Mechanical Systems, Tucson, USA, 2008. 58-61

[18] Schnakenberg U, Walter P, Vom Bögel G, et al. Initial investigations on systems for measuring intraocular pressure. *Sensors and Actuators A: Physical*, 2000, 85(1-3): 287-291

[19] Gabriel S, Lau R, Gabriel C. The dielectric properties of biological tissues: II. Measurements in the frequency range 10 Hz to 20 GHz. *Physics in medicine and biology*, 1996, 41(11): 2251

[20] Reinisch H, Gruber S, Unterassinger H, et al. An electro-magnetic energy harvesting system with 190nW idle mode power consumption for a BAW based wireless sensor node. *IEEE Journal of Solid-State Circuits*, 2011, 46(7): 1728-1741

[21] Yi J, Ki W H, Tsui C Y. Analysis and design strategy of UHF micro-power CMOS rectifiers for micro-sensor and RFID applications. *IEEE Transactions on Circuits and Systems I: Regular Papers*, 2007, 54(1): 153-166

[22] Barnett R E, Liu J, Lazar S. A RF to DC voltage conversion model for multi-stage rectifiers in UHF RFID transponders. *IEEE Journal of Solid-State Circuits*, 2009, 44(2): 354-370

[23] Papotto G, Carrara F, Palmisano G. A 90-nm CMOS threshold-compensated RF energy harvester. *IEEE Journal of Solid-State Circuits*, 2011, 46(9): 1985-1997

[24] Kotani K, Sasaki A, Ito T. High-efficiency differential-drive CMOS rectifier for UHF RFIDs. *IEEE Journal of Solid-State Circuits*, 2009, 44(11): 3011-3018

Liu Demeng, born in 1985. He is pursuing his Ph. D degrees in Shanghai Advanced Research Institute of Chinese Academy of Science. He received his B. S. and M. S. degrees from Henan University and Chinese Academy of Science in 2008 and 2011 respectively. His research interests include the design of implantable medical and low power integrated circuit.